Computational Analysis of Wetting on Hydrophobic Surfaces: Application to Self-Cleaning Mechanisms

Muhammad Osman* and Roger A. Sauer**,[1]

*Institute of Mechanics, Technical University of Dortmund, Leonhard-Euler Strasse 5, 44265 Dortmund, Germany

**Aachen Institute for Advanced Study in Computational Engineering Science (AICES), RWTH Aachen University, Templergraben 55, 52056 Aachen, Germany

Published[2] in *Advances in Contact Angle, Wettability and Adhesion, Volume 2*,
doi/10.1002/9781119117018.ch5
Submitted on 15. November 2014, Revised on 17 February 2015, Accepted on 8. June 2015

Abstract

In this work, we present a 3D model capable of describing the detailed interactions involved in self-cleaning mechanisms, which are exhibited by some hydrophobic surfaces. The model is based on a continuum mechanical formulation, and is discretized using the finite element (FE) method. A stabilized FE formulation is used to model the liquid membrane. The microstructure of the surface is modeled by spherical functions, which represent the surface asperities. When these surfaces are wetted by liquid droplets, local contact regions can be captured at the individual asperities. Generally, the contact angle which characterizes the surface has a dominant effect on the wetting behavior. Based on the presented model, the deformation of a 3D droplet in contact with a micro-structured hydrophobic surface can be computed for given droplet and surface parameters. Furthermore, the same model can be adapted to capture the interaction between the droplet and contaminant particles. Knowing the local membrane deformation at each particle, the equilibrium forces acting on the particle can be computed. This can help in providing an answer to the question: Does self-cleaning work for given droplet and particles parameters? Numerical examples are shown for two types of interactions: wetting on rough surfaces represented by spherical functions, and contact of liquid membranes with rigid spherical particles.

Keywords: Self-cleaning mechanism, contact angle, static wetting, nonlinear finite element analysis, droplet membranes.

1 Introduction

Computational treatments of wetting problems provide in many cases explanations for physical phenomena, which are difficult and sometimes even impossible to be obtained through experiments. Therefore, several numerical techniques are utilized to solve such problems, based on mathematical models. Wetting is often modeled by a system of a liquid droplet in contact with a substrate surface with a predefined contact angle. The first mathematical equation which describes the contact angle of a solid flat surface was introduced in 1805 by Young [1]. Wenzel

[1]corresponding author, email: sauer@aices.rwth-aachen.de
[2]This pdf is a personal version of an article whose final publication is available at www.onlinelibrary.wiley.com

[2] extended Young's equation to model surface roughness, considering that the liquid fills the gaps between the surface asperities, and a non-composite state exists in the contact region. The composite state, where air fills the gaps between the asperities was first proposed by Cassie and Baxter [3]. They found out that the hydrophobicity, i.e the wetting of a surface is significantly affected by the air-surface area fraction. This conclusion was enhanced by Johnson and Dettre [4] who argued that surfaces of higher roughness are more likely to be in the composite state during wetting.

The multi-scale nature of hydrophobic surfaces is mathematically modeled by Osman et al. [5] and Osman and Sauer [6] by considering superposed exponential functions with multiple levels representing different length-scales. Using the finite element method (FEM), these works studied the effect of the contact angle captured locally at the individual asperities on the wetting behavior, considering axisymmetric droplets. Investigations on the effect of surface roughness on wetting at the macro-level are provided by Raeesi et al. [7], and at the nano-level by Lee et al. [8].Kavousanakisa et al. [9] studied the patterns of surface roughness which influence the transition between Cassie-Baxter and Wenzel wetting states.

Numerically, static droplets in contact with flat surfaces were first modeled by Brown et al. [10], who derived a FE formulation to solve the Young-Laplace equation. Their Cartesian-based formulation was, however, limited to contact with flat surfaces. In order to capture complex geometries at the contact interface, it is useful to use curvilinear coordinates to describe surfaces and displacements as done by Steigmann et al. [11], and Agrawal and Steigmann [12; 13]. A general 3D model for droplets in contact with rough surfaces based on curvilinear coordinates is presented by Sauer et al. [14] and Sauer [15]. A stabilized FE formulation for static liquid membranes was used to model the droplet. Here, we employ this model to account for different contact angles representing wetting on rough surfaces. Furthermore, we use the model to describe the interactions between contaminant particles and liquid membranes, which take place in self-cleaning mechanisms. This work extends the 2D model introduced by Osman and Sauer [16], and provides a general 3D framework for modeling interactions between membrane interfaces and rigid particles. Examples shown here are limited to static contact angles, however the model can be extended to account for the contact angle hysteresis.

This paper is organized as follows: Section 2 provides a brief overview on the basic definitions used in differential geometry, on which the droplet membrane model is based. Then the model describing a self-cleaning system is illustrated in Section 3, where the following individual sub-models are introduced: the droplet model, the substrate surface model and the model discussing the particle-droplet interaction. The governing equations of these models are presented in Section 4, followed by the force analysis for the last model performed in Section 5. Numerical examples are shown in Section 6 in order to clarify the theory. In the end, we outline the summary of the presented work in Section 7.

2 Basic relations in differential geometry

Here, we briefly overview the basic definitions and relations used to describe curvilinear coordinate systems in Euclidean space. These definitions are used to derive the governing equations in Section 4. The kinematics of the membrane is also expressed in differential geometry. For further discussion on the topic refer to Carmo [17] and Kreyszig [18]. A two-dimensional surface $\mathcal{S}$ is characterized by a general set of coordinates (ξ^1, ξ^2) as shown in figure 1. The point (ξ^1, ξ^2) in the parameter domain $\mathcal{P}$ and its mapping $\boldsymbol{x}$ on the surface $\mathcal{S}$ are defined by the vector

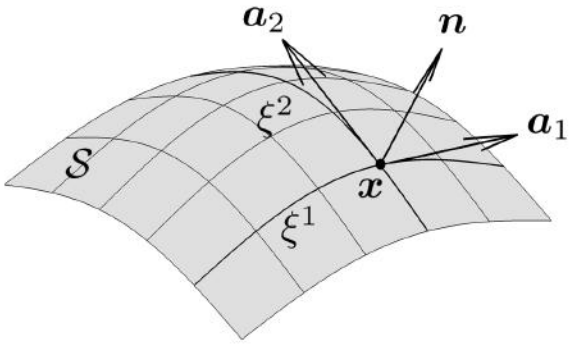

Figure 1: 2-D Surface in curvilinear coordinates

$\boldsymbol{x} = \boldsymbol{x}(\xi^1, \xi^2)$. The associated tangent vectors read

$$\boldsymbol{a}_\alpha = \frac{\partial \boldsymbol{x}}{\partial \xi^\alpha}, \quad \alpha = 1, 2. \tag{1}$$

These tangents are generally non-orthogonal and are not normalized. Greek indices take values in 1, 2, and repeated indices are summed according to index notation. Eq.(1) defines the basis for the tangent plane at $\boldsymbol{x}$, which is characterized by the metric tensor

$$a_{\alpha\beta} := \boldsymbol{a}_\alpha \cdot \boldsymbol{a}_\beta, \tag{2}$$

with the contra-variant components of the metric tensor defined by

$$a^{\alpha\beta} := [a_{\alpha\beta}]^{-1}. \tag{3}$$

The normal vector can then be defined as

$$\boldsymbol{n} = \frac{\boldsymbol{a}_1 \times \boldsymbol{a}_2}{\sqrt{\det[a_{\alpha\beta}]}}. \tag{4}$$

The contra-variant pair of tangent vectors can be defined in terms of $a^{\alpha\beta}$ as

$$\boldsymbol{a}^\alpha = a^{\alpha\beta}\boldsymbol{a}_\beta, \tag{5}$$

which satisfies $\boldsymbol{a}^\alpha \cdot \boldsymbol{a}^\beta = a^{\alpha\beta}$. Then it can be easily shown that

$$\boldsymbol{a}^\alpha \cdot \boldsymbol{a}_\beta = \delta^\alpha_\beta, \tag{6}$$

where δ^α_β is the Kronecker symbol. From the definitions of $a_{\alpha\beta}$ and $a^{\alpha\beta}$ in Eqs.(2) and (3), it follows that

$$a^{\alpha\beta}a_{\alpha\gamma} = \delta^\beta_\gamma. \tag{7}$$

The basis $\{\boldsymbol{a}^1, \boldsymbol{a}^2, \boldsymbol{n}\}$ constitutes a dual basis on the tangent plane, with $a^{\alpha\beta}$ as the dual metric. A vector $\boldsymbol{v}$ in $\mathbb{R}^3$ can then be decomposed using both bases $\{\boldsymbol{a}_1, \boldsymbol{a}_2, \boldsymbol{n}\}$ and $\{\boldsymbol{a}^1, \boldsymbol{a}^2, \boldsymbol{n}\}$ as,

$$\boldsymbol{v} = v^\beta \boldsymbol{a}_\beta + v_n \boldsymbol{n} = v_\beta \boldsymbol{a}^\beta + v_n \boldsymbol{n}, \tag{8}$$

where v_β and v^β are, respectively, the co-variant and contra-variant components of the vector

$\boldsymbol{v}$, defined as

$$v^\beta = \boldsymbol{v} \cdot \boldsymbol{a}^\beta \qquad \text{and} \qquad v_\beta = \boldsymbol{v} \cdot \boldsymbol{a}_\beta. \tag{9}$$

The co- and contra-variant components are related by

$$v^\beta = a^{\beta\alpha} v_\alpha \qquad \text{and} \qquad v_\beta = a_{\beta\alpha} v^\alpha. \tag{10}$$

Surface tensors generally take the form

$$\boldsymbol{\sigma} = \sigma^{\alpha\beta}(\boldsymbol{a}_\alpha \otimes \boldsymbol{a}_\beta) = \boldsymbol{\sigma} = \sigma_{\alpha\beta}(\boldsymbol{a}^\alpha \otimes \boldsymbol{a}^\beta). \tag{11}$$

Using Weingarten formula, the curvature tensor can be expressed in terms of the derivative of $\boldsymbol{n}$ as

$$b_{\alpha\beta} = -\boldsymbol{n}_{,\alpha} \cdot \boldsymbol{a}_\beta. \tag{12}$$

The derivative of $\boldsymbol{a}_\alpha$ can be computed from Eq.(1) as

$$\boldsymbol{a}_{\alpha,\beta} = \boldsymbol{x}_{,\alpha\beta}, \tag{13}$$

with $\boldsymbol{x}_{,\alpha\beta} = \dfrac{\partial^2 \boldsymbol{x}}{\partial \xi^\alpha \partial \xi^\beta}$. Next, we introduce the so-called co-variant derivative of $\boldsymbol{a}_\alpha$,

$$\boldsymbol{a}_{\alpha;\beta} := \boldsymbol{a}_{\alpha,\beta} - \Gamma^\gamma_{\alpha\beta} \boldsymbol{a}_\gamma. \tag{14}$$

3 System model

We consider the system model depicted in figure 2, which describes the self-cleaning mechanism through the following sub-models; (1) droplet model, (2) substrate surface model, and (3) particle-droplet interaction model. Since quasi-static conditions are considered in this work, it is convenient to treat the droplet as a hydrostatic bulk and a deformable liquid membrane. The latter is modeled using the stabilized FE formulation introduced by Sauer [15], which captures the in-plane equilibrium of the membranes due to constant surface tension. The multi-scale nature of self-cleaning surfaces can be mathematically modeled as 2D sinusoidal functions as done by Bittoun and Marmur [19], and Iliev and Pesheva [20], or as superimposed 2D exponential functions as in Osman and Sauer [6]. Here we introduce a new 3D surface model based on superimposed spherical functions, parameterized by the radii and spacings between neighboring spheres. This model represents the micro-scale level, where only one level of roughness is captured. Surface and line contact algorithms are incorporated in the liquid membrane model, in order to capture wetting on the individual asperities of the rough surface. The third model presented in this work discusses the forces acting on a rigid spherical contaminant particle interacting with the liquid membrane, in order to assess whether the contaminant particle will be lifted towards the droplet or remains attached to the substrate surface. The liquid membrane formulation used in the first model is employed here, and the contact algorithms are adapted to model the interactions with spherical rigid particles.

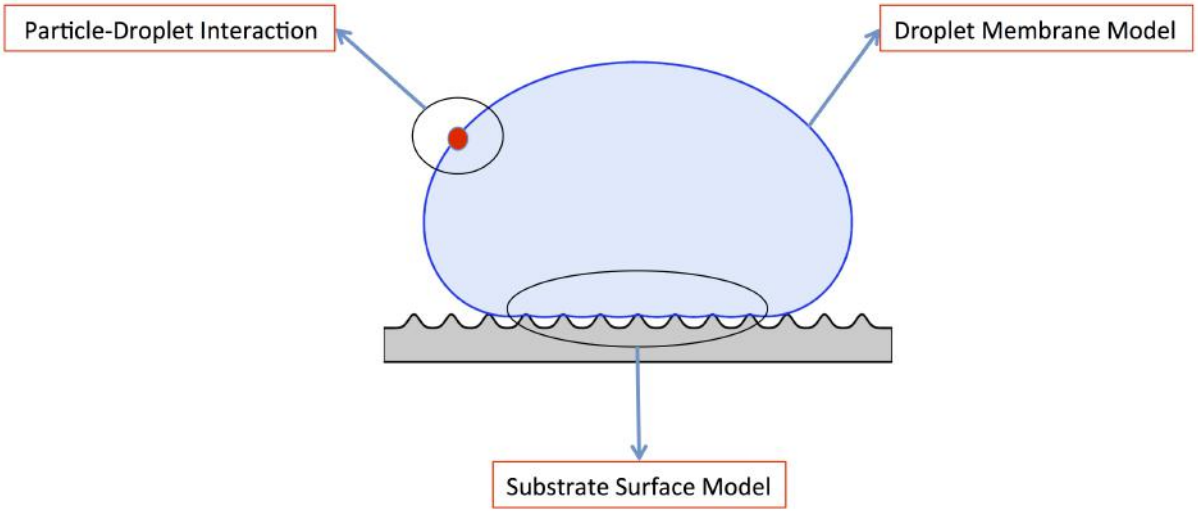

Figure 2: Self-cleaning system model comprising: droplet membrane model, substrate surface model, and particle-droplet interaction model.

4 Governing equations

4.1 Droplet membrane

The equilibrium equation of the static membrane surface $\mathcal{S}_s$ can be expressed as

$$\boldsymbol{t}^{\alpha}_{;\alpha} + \boldsymbol{f} = \boldsymbol{0}, \tag{15}$$

where $t^{\alpha}_{;\alpha}$ is the covariant derivative of the membrane traction $\boldsymbol{t}$, and $\boldsymbol{f}$ is the vector of body forces. The latter can be split into the in-plane and out-of-plane components

$$\boldsymbol{f} = f^{\alpha}\boldsymbol{a}_{\alpha} + p\boldsymbol{n}, \tag{16}$$

where f^{α} $(\alpha = 1, 2)$ are the tangential components of the traction, and p is the normal pressure. The traction on the surface, normal to $\boldsymbol{a}^{\alpha}$, can be defined in terms of the interface stress $\boldsymbol{\sigma}$ as

$$\boldsymbol{t}^{\alpha} = \boldsymbol{\sigma}\boldsymbol{a}^{\alpha}. \tag{17}$$

Substituting Eqs.(17) and (16) into (15) and performing some manipulations yields two balance equations: one in the in-plane direction,

$$\sigma^{\alpha\beta}_{;\beta} + f^{\alpha} = 0, \tag{18}$$

and the other in the out-of-plane direction

$$\sigma^{\alpha\beta}b_{\alpha\beta} + p = 0. \tag{19}$$

For liquid membranes, the surface tension is a hydrostatic stress state, $\sigma^{\alpha\beta} = \gamma a^{\alpha\beta}$, and Eq.(19) becomes the well-known Young-Laplace equation which is often written as

$$2H\gamma + p = 0, \tag{20}$$

where H denotes the mean curvature defined by $2H = b^{\alpha}_{\alpha}$, while b^{α}_{β} are the mixed components of the curvature tensor, and $b^{\alpha}_{\alpha} = b^{1}_{1} + b^{2}_{2}$. The pressure p is defined w.r.t a predefined reference level and comprises the capillary pressure p_0 and the hydrostatic pressure,

$$p = p_0 + \rho_s g u, \tag{21}$$

where u is the surface height w.r.t the reference level. The dimensionless form of Eq.(20) is obtained through dividing it by γL_0, where L_0 is a reference length,

$$2\tilde{H} = \lambda + B\tilde{u}, \tag{22}$$

where λ is the Lagrange multiplier representing the capillary pressure, $B\tilde{u}$ is the hydrostatic pressure, with $B = \rho_s g L_0^2/\gamma$ is the so-called Bond number, $\tilde{H}$ and $\tilde{u}$ are respectively the normalized curvature and surface height. ρ_s is the density of the liquid and g is the gravitational force. The covariant derivatives $\sigma^{\alpha\beta}_{;\beta}$ in Eq.(18) vanish for liquid membranes with constant surface tension, which means that Eq.(18) is trivially satisfied for arbitrary values of traction f^{α}. Physically interpreted, hydrostatic membranes do not naturally support in-plane loads. A stabilization scheme is therefore essential as a numerical treatment for the in-plane stability. Here we use the scheme proposed by Sauer [15], which substitutes $\sigma^{\alpha\beta}$ in Eq.(18) by the stabilization stress

$$\sigma^{\alpha\beta}_{sta} = \mu/J(a^{\alpha\beta}_{pre} - a^{\alpha\beta}), \tag{23}$$

where μ is the stabilization parameter, J is the Jacobian, and $a^{\alpha\beta}_{pre}$ is the metric tensor computed in the previous load step. Using this scheme requires very small load steps through which the solution is gradually reached when $\sigma^{\alpha\beta}_{sta}$ eventually vanishes, satisfying Eq.(18).

4.2 Surface Contact

In computational contact mechanics it is conventional to denote two surfaces in contact as master surface $\mathcal{S}_m$ (often a rigid surface) and slave surface $\mathcal{S}_s$ (usually the deformable surface). The 3D substrate surface $\mathcal{S}_m$ is mathematically modeled as a set of spheres representing the physical asperities. The surface is characterized by the radius of the sphere, and the spacing between the neighboring spheres. Both parameters are usually functions of the droplet radius.

We use the closest point projection technique (see Wriggers [21]) to determine contact between the membrane and the substrate surface. We consider a point $\boldsymbol{x}_c$ which lies on the membrane surface, and find its projection on the substrate surface at $\boldsymbol{x}_p$. The impenetrability constraint characterized by the gap between the two surfaces g_n then reads,

$$g_n = (\boldsymbol{x}_c - \boldsymbol{x}_p) \cdot \boldsymbol{n}_p \geq 0, \quad \forall\, \boldsymbol{x}_c \in \mathcal{S}_s, \tag{24}$$

where $\boldsymbol{x}_p$ is the closest projection of the membrane point $\boldsymbol{x}_c$ onto the substrate surface $\mathcal{S}_m$ in the direction $\boldsymbol{n}_p$, normal to $\mathcal{S}_m$.

Generally several projections of $\boldsymbol{x}_c$ might exist, and therefore an iterative solution is necessary to compute all possible projection points $\boldsymbol{x}_m$, satisfying the orthogonality condition,

$$\boldsymbol{a}_m \cdot (\boldsymbol{x}_c - \boldsymbol{x}_m) = 0, \tag{25}$$

where $\boldsymbol{a}_m$ is the surface tangent on $\mathcal{S}_m$ at $\boldsymbol{x}_m$. In order to find the closest projection point $\boldsymbol{x}_p$ among the possible solutions, a minimum distance problem has to be solved,

$$\boldsymbol{x}_p(\boldsymbol{x}_c) = \min_{\forall \boldsymbol{x}_m \in \mathcal{S}_m} (\boldsymbol{x}_c - \boldsymbol{x}_m), \quad \forall\, \boldsymbol{x}_c \in \mathcal{S}_s. \tag{26}$$

Since the substrate surface here is represented by spheres, the projection $\boldsymbol{x}_p$, the normal $\boldsymbol{n}_p$ and the gap g_n can be explicitly determined without any further iterative steps. Knowing the position of the center of the sphere $\boldsymbol{r}_0$, we can define the normal $\boldsymbol{n}_p$ as

$$\boldsymbol{n}_p = \frac{\boldsymbol{x}_c - \boldsymbol{r}_0}{\|\boldsymbol{x}_c - \boldsymbol{r}_0\|}. \tag{27}$$

The projection $\boldsymbol{x}_p$ on the sphere of radius r_s simply lies on the line connecting the center of the sphere and the point $\boldsymbol{x}_c$, and can be defined as

$$\boldsymbol{x}_p = \boldsymbol{r}_0 + r_s \boldsymbol{n}_p. \tag{28}$$

4.3 Line contact

Wetting is mainly characterized by the contact angle formed at the liquid and solid interfaces at the contact line $\mathcal{L}_c$, the location at which the three phases meet. In this study, we distinguish two different contact interfaces; 1) the liquid membrane with the substrate surface with contact angle θ_c, and 2) the liquid membrane with the contaminant particle with contact angle θ_p. In both cases, the location of the contact line in a quasi-static framework is maintained by the balance of the interfacial tractions $\boldsymbol{t}_{SG}$, $\boldsymbol{t}_{LG}$ and $\boldsymbol{t}_{SL}$ at the solid-gas, liquid-gas and solid-liquid interfaces, respectively, through

$$\boldsymbol{t}_{SG} + \boldsymbol{t}_{LG} + \boldsymbol{t}_{SL} + \boldsymbol{q}_n = \boldsymbol{0}, \tag{29}$$

where $\boldsymbol{q}_n = q_n \boldsymbol{n}_c$ is the line load which counterbalances the projection of $\boldsymbol{t}_{LG}$ onto the normal direction $\boldsymbol{n}_c$ w.r.t $\mathcal{S}_m$. These tractions are illustrated in figure 3 which depicts one quarter of a droplet resting on a flat surface with contact angle θ_s. Both tractions $\boldsymbol{t}_{SG}$ and $\boldsymbol{t}_{SL}$ have opposite directions along the vector $\boldsymbol{m}_c$ which is normal to the surface tangent $\boldsymbol{a}_c$ and lies on the surface $\mathcal{S}_m$. The force $\boldsymbol{t}_{LG} = \gamma_{LG} \boldsymbol{a}_m$ is tangent to the liquid membrane at the plane which forms the contact angle θ_c with the master surface $\mathcal{S}_m$. The normal and tangential components of Eq.(29) w.r.t $\mathcal{S}_m$, respectively read

$$\gamma_{SG} - \gamma_{LG} \cos\theta - \gamma_{SL} = 0, \tag{30}$$

$$q_n - \gamma_{LG} \sin\theta = 0, \tag{31}$$

where γ_{SG}, γ_{LG} and γ_{SL} are the interfacial tensions at the respective interfaces. We note here that $\gamma_{LG} = \gamma$ is used in Section 4.1. The above equations hold for interactions on both substrate surfaces $\theta = \theta_c$ and contaminant particles $\theta = \theta_p$. Computationally, the contact angle θ is imposed within the membrane as a kink by applying a certain load $\boldsymbol{q}_c$ at the contact line,

$$\boldsymbol{q}_c = q_n \boldsymbol{n}_c + \gamma_{SG} \boldsymbol{m}_c. \tag{32}$$

This load $\boldsymbol{q}_c$ has to balance the tractions $\boldsymbol{t}_{LG}$ and $\boldsymbol{t}_{SL}$ (see figure 3). Therefore, computing $\boldsymbol{q}_c$ requires determining the vectors $\boldsymbol{n}_c, \boldsymbol{a}_c$, and $\boldsymbol{m}_c$. The normal $\boldsymbol{n}_c$ is computed w.r.t to the known substrate surface at the contact point, by considering the closest point projection as mentioned

in the surface contact, while the tangent $\boldsymbol{a}_c$ is determined at the membrane point $\boldsymbol{x}_c$ as

$$\boldsymbol{a}_c = \frac{\partial \boldsymbol{x}_c}{\partial \xi}. \tag{33}$$

The vector $\boldsymbol{m}_c$ is the cross-product of $\boldsymbol{a}_c$ and $\boldsymbol{n}_c$, defined as

$$\boldsymbol{m}_c = \frac{\boldsymbol{a}_c \times \boldsymbol{n}_c}{\|\boldsymbol{a}_c \times \boldsymbol{n}_c\|}. \tag{34}$$

For further details we refer to Sauer [15].

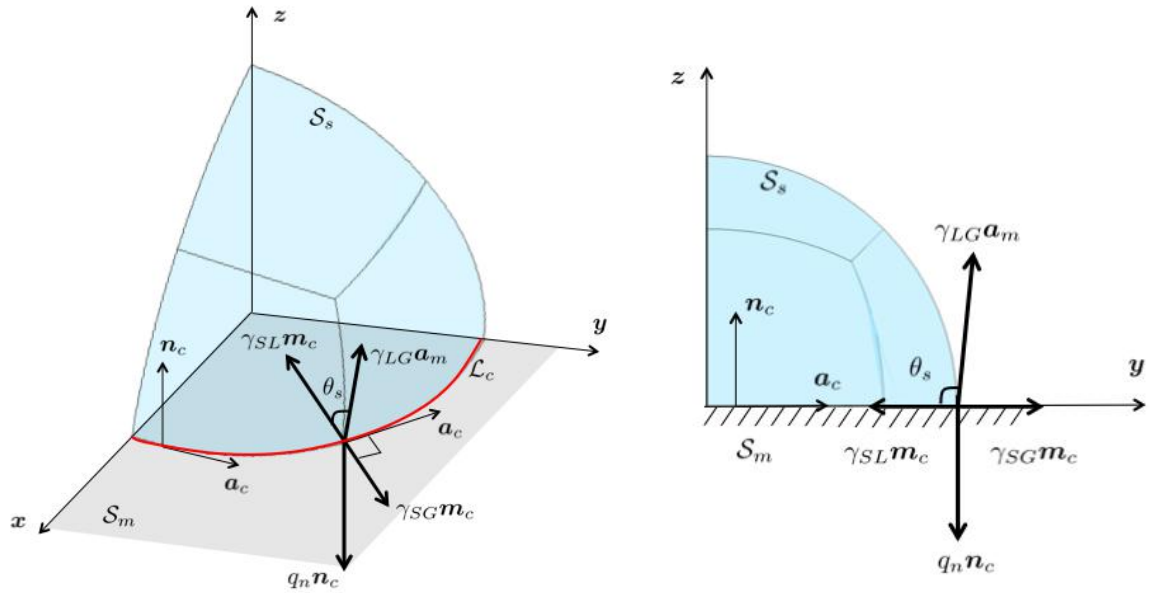

Figure 3: Forces along the contact line: (a) 3D view, and (b) 2D side-view.

5 Force analysis

We consider a rigid spherical contaminant particle of radius r_p and density ρ_p initially resting on a substrate surface and interacting with a liquid droplet under quasi-static conditions (see figure 4). Four forces are involved in this interaction: particle weight $\mathbf{F}_G$, contact line force $\mathbf{F}_{CL}$, hydrostatic force $\mathbf{F}_H$, and buoyancy force $\mathbf{F}_B$, defined as follows:

$$\mathbf{F}_G = \frac{4}{3}\pi r_p^3 \rho_p \mathbf{g}, \tag{35}$$

$$\mathbf{F}_{CL} = \oint_{\mathcal{L}_c} \boldsymbol{t}_{LG}\, \mathrm{d}\mathcal{L}_c, \tag{36}$$

$$\mathbf{F}_H = \int_{A_s} p\, \mathbf{n}\, \mathrm{d}A_s \approx p_0 A_s \mathbf{N}, \quad A_s = 2\pi r b, \tag{37}$$

$$\mathbf{F}_B = \rho_s g \mathcal{V}_s \mathbf{N}, \quad \mathcal{V}_s = \frac{\pi b}{6}(3a^2 + b^2), \tag{38}$$

where $\mathbf{n}$ is the normal to the wetted area A_s, while $\mathcal{V}_s$ is the wetted volume of the particle, $\mathbf{N}$ is the normal to the contact line along the particle axis, and $a \,\&\, b$ are distances defined in figure 4. In order to define $\boldsymbol{F}_{CL}$, the traction $\boldsymbol{t}_{LG}$ is computed from Eq.(29). The effective force $\mathbf{F}_e$ is the summation of all forces,

$$\boldsymbol{F}_e = \boldsymbol{F}_G + \boldsymbol{F}_{CL} + \boldsymbol{F}_H + \boldsymbol{F}_B. \tag{39}$$

The vertical component of $\mathbf{F}_e$ determines whether the particle is pulled upwards towards the droplet or not. In case a contact angle hysteresis evolves, the dynamic contact angles can be obtained through the tangential equilibrium, i.e the in-plane component of $\mathbf{F}_e$.

Among the above parameters, the following require computation of the membrane deformation: (1) the location of the contact line $\mathcal{L}_c$ w.r.t the particle (represented by the distances $a \,\&\, b$), (2) the traction along the liquid-gas interface $\mathbf{t}_{LG}$, and (3) the internal pressure p_0. Friction and surface adhesion between the particle and the substrate are not considered in this work. The example shown in figure 4 represents a special case of the general model depicted in figure 2 where the contaminant particle can be initially located anywhere on the droplet surface.

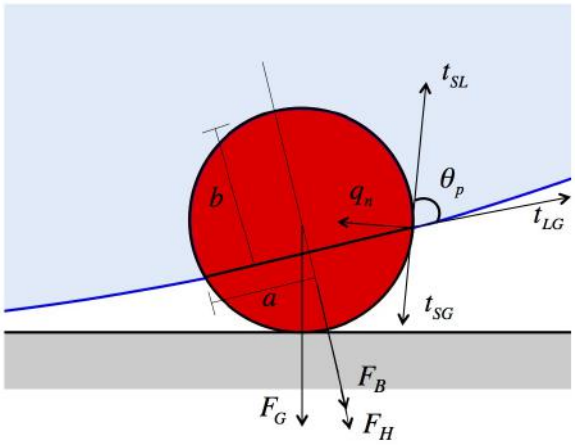

Figure 4: Schematic of the forces acting on a particle resting on a flat substrate surface, and in contact with a liquid droplet (Osman and Sauer [16]).

6 Results and Discussion

Based on the sub-models described above, we present two numerical examples: (1) wetting of droplets on a rough surface, and (2) adhesion of contaminant particles to a droplet surface. Quasi-static conditions are considered in both examples. We distinguish the parameters for the substrate surface in the first example $(\theta_s, \gamma_{SL}|^s, \gamma_{SG}|^s, \gamma_{LG}, V_s, \rho_s)$, from those for the particle in the second example $(\theta_p, \gamma_{SL}|^p, \gamma_{SG}|^p, \gamma_{LG}, V_p, \rho_p)$. It shall be noted here that the interfacial tension $\gamma_{SL}|^s$ is not necessarily the same as $\gamma_{SL}|^p$.

6.1 Wetting on Rough surface

Superhydrohobic surfaces are characterized by a liquid contact angle $\theta_s \geq 150$. This angle is locally captured at the individual asperities at the micro-scale, where the surface roughness

can be visualized. For a flat surface, however, only one global contact angle is observed. In order to distinguish between the two, we consider the examples shown in figures 5, 6, and 7 for a droplet in contact with a flat surface with $\theta_s = 180$, rough surface with $\theta_s = 180$ and with $\theta_s = 150$, respectively. Load-driven conditions are considered here, where the applied load is simply the gravity $\rho_s g = 2\gamma/2R^2$, where R is the undeformed droplet radius. The radii of the spheres representing the surface roughness $r_s = 0.05R$, and the distance between each two neighboring asperities $\triangle x = 0.2R$. As discussed in Section 4.1, numerical instability problems appear while modeling liquid membranes since they do not naturally equilibrate in-plane loads. Therefore, the stabilized finite element formulation introduced by Sauer [15] is employed to model the membrane. The stabilization parameter $\mu = \gamma$ is used in the computations. The penalty parameter used for applying the surface contact constraint is $\epsilon_n = 10^4\gamma/R$.

As observed in figures 5, 6, and 7, there is almost no change in the overall droplet deformation due to changing the roughness parameters and the contact angle. Decreasing the contact angle below 150° eventually will lead to a complete wetting (Wenzel state) of the surface, for the given surface parameters. Furthermore, the global contact angle is almost 180° in the three cases, although different local contact angles are captured at the rough surfaces in figures 6 and 7. This means that the wetting behavior of superhydrophobic surfaces is independent of the contact angle, as long as the latter is sufficiently large (about 150° in this example), and under partial wetting state (Cassie-Baxter). This observation is only valid when the surface roughness parameters are relatively small compared to the droplet size.

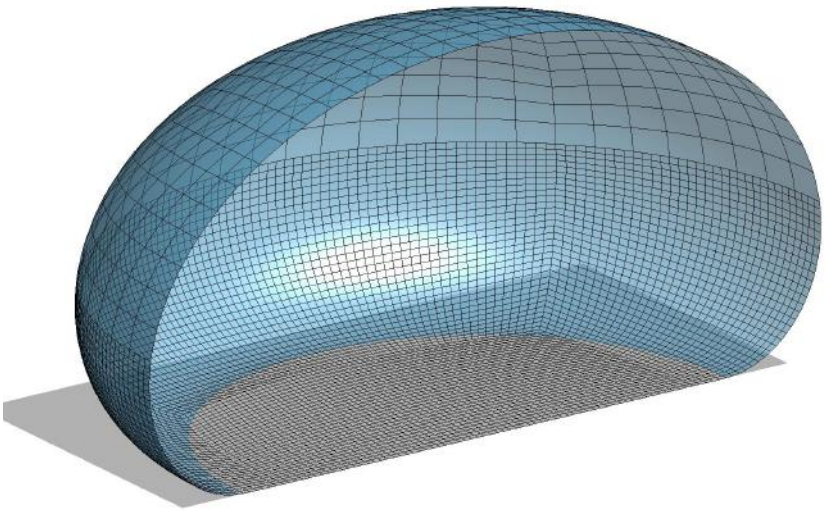

Figure 5: FE solution for a droplet in contact with a flat surface, $\theta_s = 180°$.

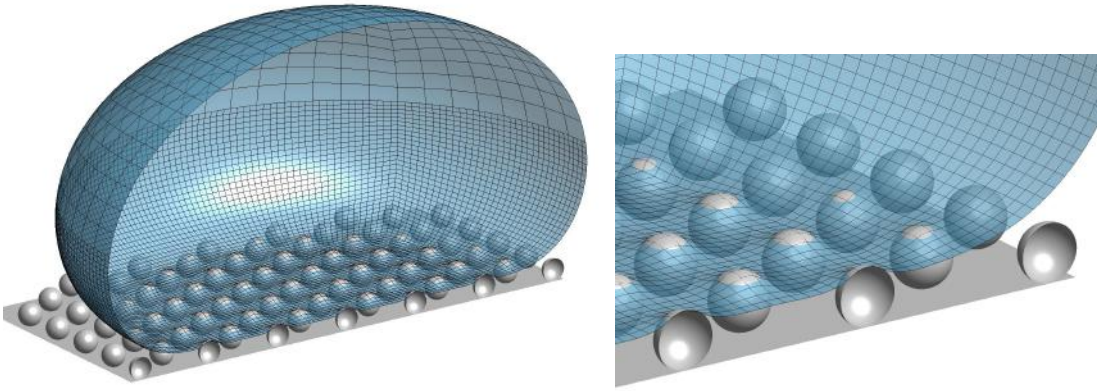

Figure 6: Left: FE solution for a droplet in contact with a rough surface, $\theta_s = 180°$. Right: zoom in.

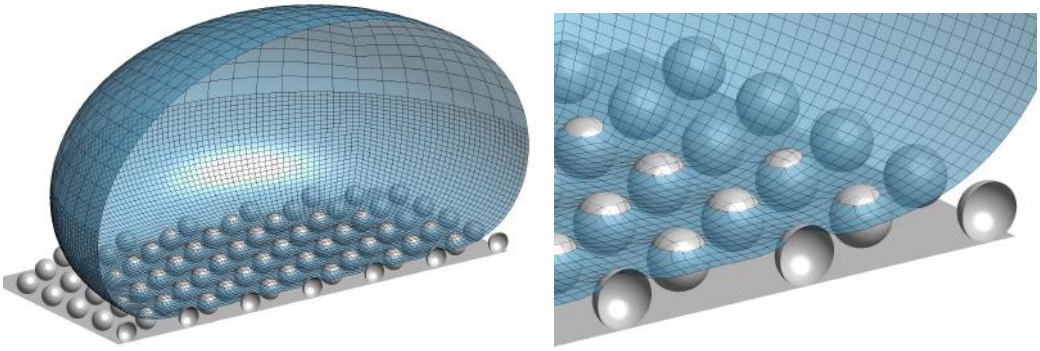

Figure 7: Left: FE solution for a droplet in contact with a rough surface, $\theta_s = 150°$. Right: zoom in.

6.2 Adhesion between droplet surface and a contaminant particle

In self-cleaning applications, contaminant particles are usually so small compared to the liquid droplet such that the surface of the droplet appears almost planar to the particle. This allows reducing the model to a simple square sheet representing the initial configuration of a liquid membrane. In order to avoid boundary effects, the dimensions of the membrane are considered to be large enough so that the undeformed membrane surface at the boundary is approximately flat. An interacting contaminant particle is represented by a sphere of radius r_p, as in figure 8. The membrane can thus be considered fixed at the boundaries. The capillary pressure effect can still be considered in this model by applying a volume constraint on the membrane (Sauer [15]).

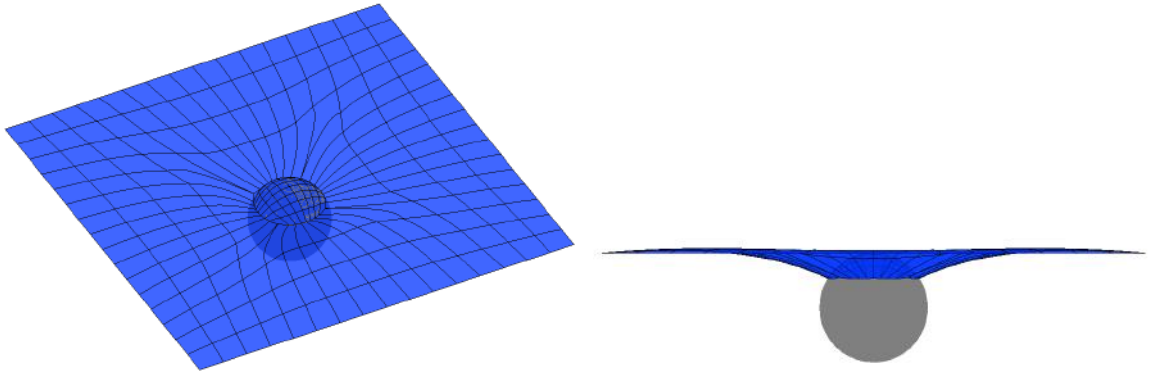

Figure 8: Left: 3D view of an FE solution for a liquid membrane in contact with a spherical rigid particle with contact angle $\theta_p = 90°$. Right: 2D side-view.

Now we employ this model to compute the membrane deformation due to contact with a spherical particle considering a predefined contact angle θ_p. Based on this deformation, we can compute the unknown parameters discussed in Section 5, and evaluate the equilibrium forces. In the following example, we consider a square membrane of dimensions $5L_0 \times 5L_0$, in contact with a rigid sphere of radius $r_p = L_0$ (see figure 9). The membrane is deformed under the distributed contact line load $\boldsymbol{q}_c$ defined in Eq.(32), applied along the contact line. Due to the symmetry of the system, it is enough to run the computations for one quarter of the system, after applying the appropriate boundary conditions. Furthermore, we assume the plane formed by the closed contact line to be horizontal. This assumption is, however, only limited to this example and not to the equations in Section 5, which are applied to any orientation of the contact line.

Figure 10 shows the membrane deformation for contact with spheres of contact angles $\theta_p = 150°, 120°, 90°$ and $30°$. Larger deformations are noticed for lower contact angles, where the net contact line force $\boldsymbol{F}_{CL}$ points inwards, pulling the sphere towards the liquid membrane. This result agrees with the physical fact that droplets tend to stick to hydrophilic surfaces through maximizing the area of contact. On the other hand, hydrophobic spheres are subjected to repulsive contact line forces pushing them away from the liquid membrane. Based on the obtained results, the forces in Eqs.(36,37) and (38) are computed, and the effective force $\boldsymbol{F}_e \cdot \boldsymbol{e}_3$ is plotted in figure 11 for spheres of different contact angles. The region where $\boldsymbol{F}_e \cdot \boldsymbol{e}_3$ is below zero in figure 11 means that the effective force is not enough to lift the sphere towards the liquid membrane. However, the positive values of $\boldsymbol{F}_e \cdot \boldsymbol{e}_3$ indicate a lift off since the contact line force overcomes the other forces. The point at which the effective force flips direction is denoted in figure 11 as a critical point. This indicates when the self-cleaning is activated and the contaminant particle is attached to the droplet. It is important to note here that the direction of the contact line force, plotted in figure 10, is not necessarily the direction of the effective force, since the other forces ($\boldsymbol{F}_H, \boldsymbol{F}_G$, and $\boldsymbol{F}_B$) pointing downwards might dominate, depending on the sphere and membrane parameters. In the above computations the density of the particle ρ_p is chosen to be the same as the density of the liquid ρ_s. Different results can be obtained for different sizes and densities of the spherical particle.

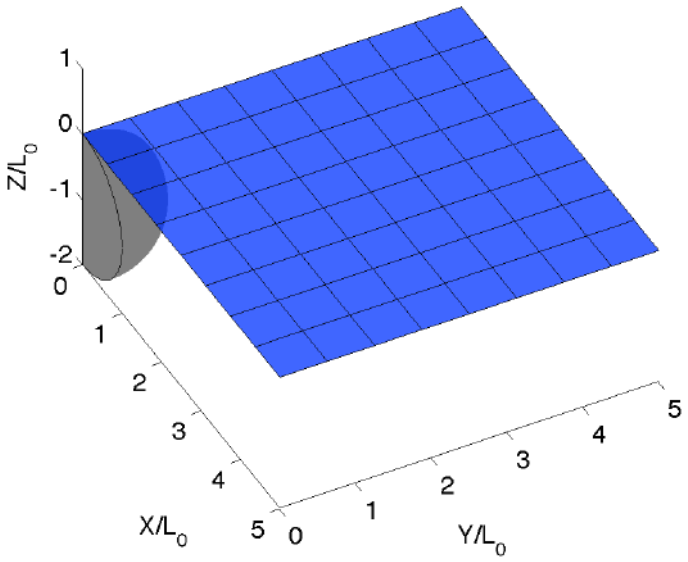

Figure 9: Initial configuration of a liquid membrane sheet in contact with a rigid sphere with contact angle $\theta_p = 180°$. Dimensions are normalized by the characteristic length L_0.

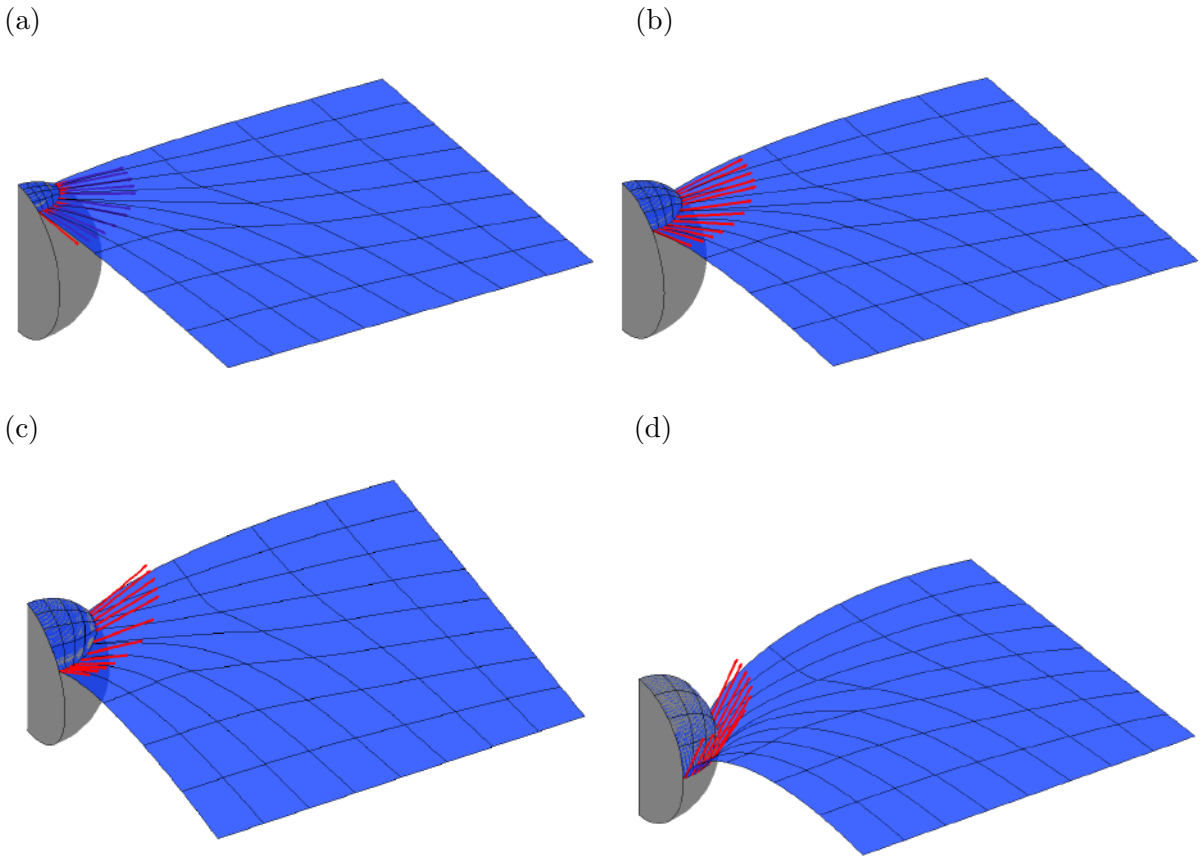

Figure 10: FE solution of a deformed liquid membrane in contact with a sphere of contact angle (a) to (d): $\theta_p = 150°, 120°, 90°$, and $30°$. The red arrows represent the directions of the distributed contact line traction $\boldsymbol{t}_{LG}$.

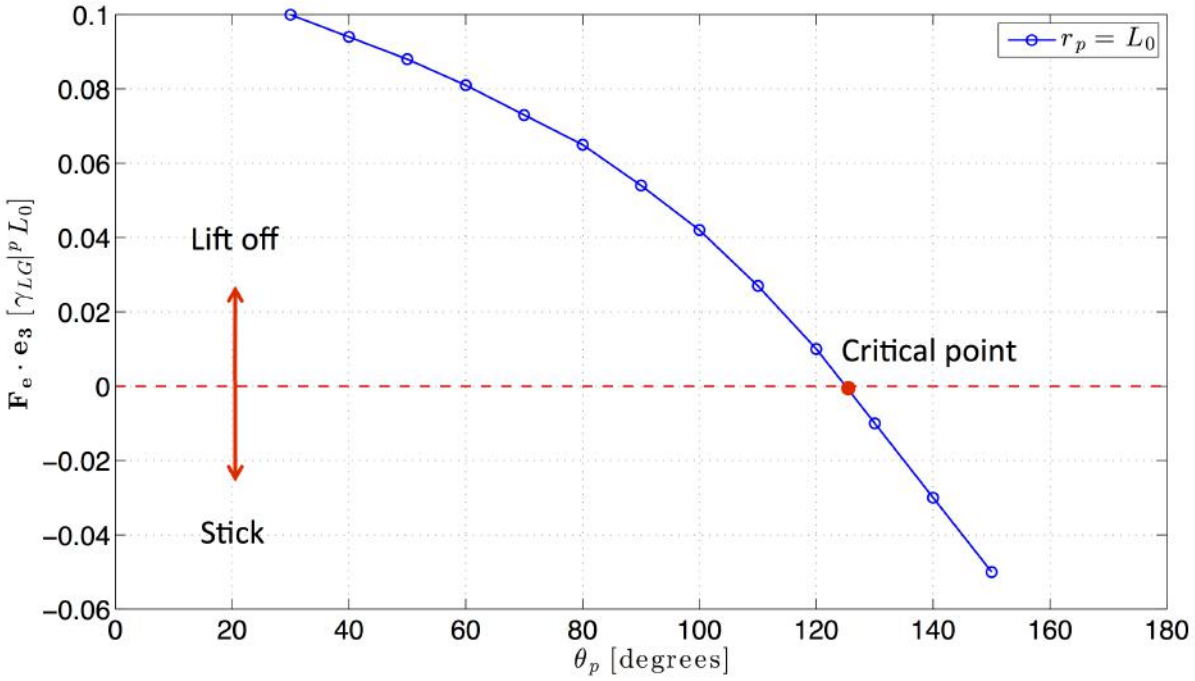

Figure 11: Effect of contact angle on the equilibrium force of particles with radii $r_p = L_0$.

The precision of the computations depends on the number of load steps taken over the contact angle. Detailed discussion on convergence of the numerical scheme used here can be found in Sauer [15]. Penetrations of the liquid membrane into the rigid surface are observed in the contact regions in figures 5, 6, 7, 8 and 10 due to the use of the penalty method, which is an approximation method. This problem can be eliminated by using other exact methods to enforce the surface contact constraint, which significantly increase the computational cost.

7 Conclusions

Static wetting of hydrophobic surfaces considering surface roughness is computationally studied through an introduced 3D model based on FEM. The same model is adapted to describe the interactions between contaminant particles and droplet surfaces, which are involved in self-cleaning mechanisms. These interactions are analyzed thorough a force balance to determine whether a contaminant particle in contact with a liquid surface will be lifted off towards it or sticks to the substrate. The force balance shows that the net contact line force is dominant for relatively small particles w.r.t the droplet. Examples shown in Section 6.2 help in explaining the self-cleaning effect through the introduced model. Furthermore, it is shown that superhydrophobicity is attainable for surfaces with sufficiently large contact angles (approximately 150°), as long as Cassie-Baxter wetting state exists. Such an independence from the contact angle can help in reducing the structural requirements while fabricating artificial superhydrophobic surfaces.

Acknowledgement

The authors are grateful to the German Research Foundation (DFG) for supporting this research under projects SA1822/3-2 and GSC 111.

References

[1] T. Young, An essay on the cohesion of fluids, *Phil. Trans. R. Soc. Lond.* 95, 65-87 (1805).

[2] R.N. Wenzel, Resistance of solid surfaces to wetting by water, *Ind. Eng. Chem.* 28, 988-994 (1936).

[3] A.B.D. Cassie and S. Baxter, Wettability of porous surfaces, *Trans. Faraday Soc.* 40, 546-551 (1944).

[4] R.E. Johnson and R.H. Dettre, Contact angle hysteresis study of an idealized rough surface, *Adv. Chem. Ser.* 43, 112-135 (1964).

[5] M. Osman, R. Rasool, and R. A. Sauer, Computational aspects of self-cleaning surface mechanisms, in: *Advances in Contact Angle, Wettability and Adhesion*, Vol.1, K.L. Mittal (Ed.), pp. 109-130, Wiley-Scrivener, Bevarly MA (2013).

[6] M. Osman and R. A. Sauer, A parametric study of the hydrophobicity of rough surfaces based on finite element computations, *Colloids Surf., A* 461, 119-125 (2014).

[7] B. Raeesi, N.R. Morrow, and G.Mason, Effect of surface roughness on wettability and displacement curvature in tubes of uniform cross-section, *Colloids Surf., A* 436, 392-401 (2013).

[8] S.M. Lee, I.D. Jung, and J.S. Ko, The effect of the surface wettability of nanoprotrusions formed on network type microstructures, *J. Micromech. Microeng.* 18, 125007 (7pp) (2008).

[9] M.E. Kavousanakisa, C.E. Colosquib, and A.G. Papathanasiou, Engineering the geometry of stripe-patterned surfaces toward efficient wettability switching, *Colloids Surf., A* 436, 309-317 (2013).

[10] R.A. Brown, F.M. Orr, and L.E. Scriven, Static drop on an inclined plate: Analysis by the finite element method, *J. Colloid Interface Sci.* 73, 76-87 (1980).

[11] D. Steigmann, E. Baesu, R.R. Rudd, J. Belak, and M. McElfresh, On the variational theory of cell-membrane equilibria, *Interface Free Bound.* 5, 357-366 (2003).

[12] A. Agrawal and D.J. Steigmann, Modeling protein-mediated morphology in biomembranes, *Biomech. Model Mechanobiol.* 8, 371-379 (2009).

[13] A. Agrawal and D.J. Steigmann, Boundary value problems in the theory of lipid membranes, *Continuum Mech. Thermodyn.* 21, 57-82 (2009).

[14] R. A. Sauer, X.T. Duong, and C.J. Corbett, A computational formulation for constrained solid and liquid membranes considering isogeometric finite elements, *Comput. Method Appl. Mech. Engrg.* 271, 48-68 (2014).

[15] R. A. Sauer, Stabilized finite element formulations for liquid membranes and their application to droplet contact, *Int. J. Numer. Meth. Fluids* 75, 519-545 (2014).

[16] M. Osman and R. A. Sauer, Quasi-static analysis of self-cleaning surface mechanisms, in Proceedings of the 22nd UK Conference on Computational Mechanics (ACME2014), pp. 324-327 (2014).

[17] M.P. Do Carmo, *Differential Geometry of Curves and Surfaces*, Prentice-Hall (1976).

[18] E. Kreyszig, *Differential Geometry*, Dover (1991).

[19] E. Bittoun and A. Marmur, The role of multiscale roughness in lotus effect: Is it essential for super-hydrophobicity?, *Langmuir* 28, 13933-42 (2012).

[20] S. Iliev and N. Pesheva, Nonaxisymmetric drop shape analysis and its application for determination of local contact angles, *J. Colloid Interface Sci.* 301, 677-684 (2006).

[21] P. Wriggers, *Computational Contact Mechanics*, 2nd ed. Springer, Germany (2006).